

PointSlice: Accurate and Efficient Slice-Based Representation for 3D Object Detection from Point Clouds

Liu Qifeng, Zhao Dawei, Dong Yabo, Xiao Liang, Wang Juan, Min Chen, Li Fuyang,
Jiang Weizhong, Lu Dongming, Nie Yiming

^a*Zhengjiang University, College of Computer Science and Technology, Hangzhou,
Zhejiang, 310058, Zhejiang, China*

^b*Defense Innovation Institute, Beijing, 100000, Beijing, China*

^c*Tsinghua University, Department of Computer Science and Technology, Beijing, 100000, Beijing, China*

Abstract

3D object detection from point clouds plays a critical role in autonomous driving. Currently, the primary methods for point cloud processing are voxel-based and pillar-based approaches. Voxel-based methods offer high accuracy through fine-grained spatial segmentation but suffer from slower inference speeds. Pillar-based methods enhance inference speed but still fall short of voxel-based methods in accuracy. To address these issues, we propose a novel point cloud processing method, PointSlice, which slices point clouds along the horizontal plane and includes a dedicated detection network. The main contributions of PointSlice are: (1) A new point cloud processing technique that converts 3D point clouds into multiple sets of 2D (x-y) data slices. The model only learns 2D data distributions, treating the 3D point cloud as separate batches of 2D data, which reduces the number of model parameters and enhances inference speed; (2) The introduction of a Slice Interaction Network (SIN). To maintain vertical relationships across slices, we incorporate SIN into the 2D backbone network, which improves the model’s 3D object perception capability. Extensive experiments demonstrate that PointSlice achieves high detection accuracy and inference speed. On the Waymo dataset, PointSlice is $1.13\times$ faster and has $0.79\times$ fewer parameters than the state-of-the-art voxel-based method (SAFDNet), with only a 1.2 mAPH accuracy reduction. On the nuScenes dataset, we achieve a state-of-the-art detection result of 66.74 mAP. On the Argoverse 2 dataset, PointSlice is $1.10\times$ faster, with $0.66\times$ fewer parameters and a 1.0 mAP accuracy reduction. The code will be available at

<https://github.com/qifeng22/PointSlice2>.

Keywords: point cloud, 3D object detection, slice representation

1. Introduction

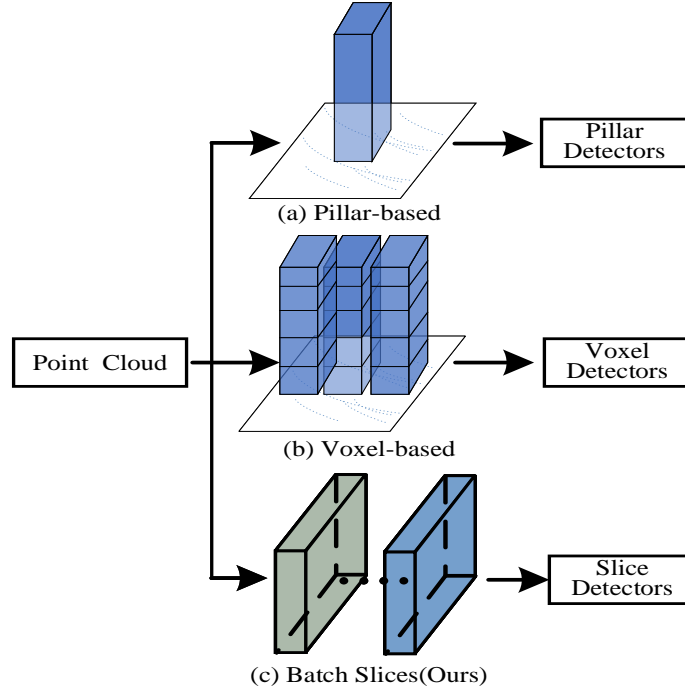


Figure 1: Comparison of different point cloud processing methods: pillar-based, voxel-based, and batch slices (Ours).

LiDAR-based 3D object detection has been extensively studied due to its applications in autonomous driving and robotics [1]. The inherent sparsity and uneven spatial distribution of point clouds make it challenging to directly apply 2D image network architectures to point cloud data. To address these characteristics, the mainstream approach for processing point clouds is voxelization. The two primary voxelization methods are voxel-based and pillar-based approaches (see fig. 1). Voxel-based methods divide the point cloud space into a 3D voxel grid; models such as HEDNet [2] and SAFDNet [3] utilize hierarchical encoder-decoder architectures and sparse detection

head structures, achieving outstanding detection performance. However, voxel-based approaches require learning in the x, y, and z dimensions, which results in slower inference speeds compared to pillar-based methods. Pillar-based methods compress the point cloud data into the x-y plane, reducing input dimensionality and thus improving inference efficiency. For instance, PillarNet [4] employs spatial feature semantic fusion to further enhance detection accuracy. Given the efficiency advantages of the pillar-based approach, a natural question arises: can the voxel-based network structure be directly applied to point clouds initialized in a pillar format? We conducted experiments on the Waymo Open dataset to explore this question. As shown in table 1, although using pillar-formatted point clouds (SAFD-Pillar) results in an inference speed $1.17\times$ faster than SAFDNet, it achieves only 69.3 mAPH in detection accuracy.

Method	mAPH(L2)	Params	Speedup	FPS
SAFDNet	73.9	9.89M	1.0 \times	13.68
SAFD-Pillar	69.3	7.74M	1.17 \times	15.95

Table 1: Comparison of pillarization results for SAFDNet[3] on the Waymo validation set.

To address the issue of improved efficiency but reduced detection accuracy, we propose PointSlice, which converts 3D point cloud data into multiple (x-y) slices, allowing the model to maintain detection accuracy close to that of voxel-based methods. PointSlice introduces a novel encoding approach: we partition the point cloud horizontally, transforming 3D data into a set of 2D slices, where the neural network does not differentiate between the heights (z positions) of the slices. This set of 2D slices is treated as a batch. Through this encoding, PointSlice can utilize a 2D convolutional network as the backbone for feature extraction, thereby overcoming the inefficiency of voxel-based methods that require 3D CNNs for inference.

However, due to the relationships among different slices of the same point cloud, solely learning from individual 2D slices would likely compromise the model’s final detection performance, as shown in the ablation studies. To address this, we further introduce the Slice Interaction Network (SIN), which incorporates sparse 3D convolu-

tions within the 2D backbone network to enable information exchange across slices. Since SIN is composed of 3D convolutions, excessive use would increase model parameters and reduce inference efficiency. Therefore, we carefully add SIN only where necessary to preserve detection accuracy. Experimental results validate the importance of the SIN network.

To validate the effectiveness of our model, we conducted experiments on the Waymo and nuScenes datasets. On the Waymo dataset, our model achieves an inference speed that is $1.13\times$ faster than the state-of-the-art voxel-based method (SAFDNet), with $0.79\times$ fewer parameters. On the nuScenes dataset, our model demonstrates $0.45\times$ fewer parameters than SAFDNet, while achieving a state-of-the-art detection result of 66.74 mAP.

Overall, the contributions of this paper are as follows:

- (1) we propose a novel representation that converts 3D point clouds into 2D slices;
- (2) we design a dedicated network structure, PointSlice, which innovatively incorporates the Slice Interaction Network (SIN);
- (3) we demonstrate the efficiency and high accuracy of our model on the Waymo, nuScenes, and Argoverse 2 datasets.

2. Related work

2.1. Voxel-based 3D detectors

Voxel-based detection networks divide point cloud data into 3D voxel grids and utilize neural networks for 3D object detection. VoxelNet [5] divides the point cloud into evenly spaced 3D voxels and converts each point cluster within a voxel into a unified feature representation through the Voxel Feature Encoding (VFE) layer. Voxel R-CNN [6] achieves precise object localization by fully leveraging voxel features within a two-stage approach. TransFusion [7] introduces a Transformer decoder-based detection head. HEDNet [2] proposes a hierarchical encoder-decoder network for 3D object detection, employing encoder-decoder blocks to capture long-range dependencies between features in space, particularly for large and distant objects. These methods have

progressively improved detection accuracy, but inference efficiency remains a challenge.

To address the issue of inference efficiency, several works have explored solutions [8, 9]. VoxelNeXt[10] introduced a fully sparse detection network with a sparse detection head, addressing the inefficiency in prior voxel-based networks that required sparse features to be converted into dense feature maps. This conversion reduced inference efficiency. SAFDNet[3] further improved the sparse detection head by designing an adaptive feature diffusion strategy to address the issue of missing central features for detected objects, achieving state-of-the-art detection results while ensuring high inference efficiency. However, even with fully sparse detectors, voxel-based methods still lag behind the upcoming pillar-based methods in terms of inference efficiency.

2.2. Pillar-based 3D detectors

Pillar-based methods [11, 12] build upon voxel-based approaches to further enhance the model’s deployment feasibility in practical applications. PointPillars [12] represents point clouds as vertical columns (pillars) and uses a 2D convolutional detection architecture for object detection. CenterPoint [13] improves the accuracy of pillar-based methods by employing a keypoint detector to identify object centers. PillarNet [4] further proposes a neck network with spatial semantic feature fusion. [14] proposed a hybrid Voxel-Pillar Fusion network (VPF), which combines the strengths of voxel and pillar representations. They developed a sparse voxel-pillar encoder using 3D and 2D sparse convolutions and introduced a Sparse Fusion Layer (SFL) to enable bidirectional interaction between voxel and pillar features. Although these studies have continuously improved the detection accuracy of pillar-based methods, a gap remains when compared to the advancing voxel-based methods.

To address the limitations of both types of detectors, we propose a novel point cloud encoding method PointSlice, which slices the point cloud horizontally and employs a Slice Interaction Network (SIN) to enable efficient and accurate 3D object inference.

3. PointSlice

3.1. Background

Sparse convolutions. Sparse convolution is a convolutional operation developed specifically for sparse data, operating only on locations where data exists. This approach enhances computational efficiency and reduces memory usage. Sparse convolution is mainly divided into two types: submanifold sparse convolution (subm spconv) [15], which maintains feature sparsity between input and output feature maps, and regular sparse convolution [16], which increases feature map density by expanding features into neighboring areas, further filling the sparse space. In our Slice Interaction Network (SIN) module, we employ both types of convolution for information exchange between slices.

Sparse encoder-decoder block (EDB). HEDNet [2] proposes merging sparse encoder-decoder blocks that capture long-range dependencies between features while maintaining computational efficiency.

Sparse detection head. Sparse detection heads primarily address the redundant computations associated with dense feature maps. SAFDNet [3] maintains feature sparsity throughout the entire detection process, while its proposed Adaptive Feature Diffusion (AFD) strategy mitigates the issue of missing central features, enabling fully sparse detection networks to achieve higher accuracy.

3.2. Overall architecture

fig. 2 illustrates the overall architecture of the PointSlice model, which operates in three stages: (1) transforming the point cloud into multiple sets of 2D slices; (2) extracting slice features through a sparse backbone, where the Slice Interaction Network (SIN) enables efficient information exchange across slices; and (3) performing final detection via a sparse detection head.

3.2.1. Point cloud to Slices

Given a set of point cloud data with a shape of $(B, N, 3)$, where B denotes the batch size, N represents the number of points in each point cloud (assuming each frame has an identical number of points), 3 corresponds to the spatial coordinates (x, y, z) . Initially,

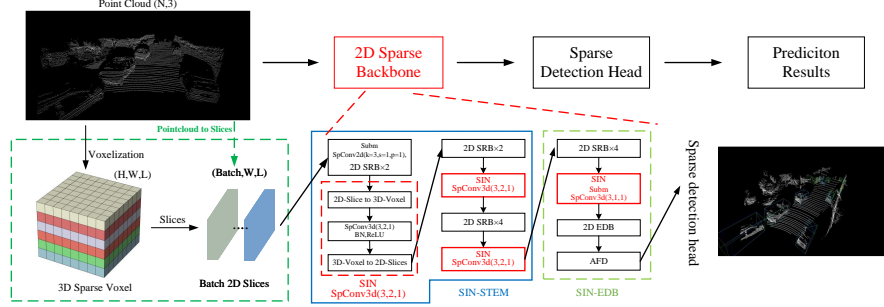


Figure 2: Overall framework of PointSlice. The dashed boxes labeled ‘Pointcloud to Slice’ and ‘Slice Interaction Network (SIN)’ represent the main contributions of this paper. The raw point clouds, after voxelization and slicing, are input into a 2D backbone network for feature extraction. The 2D backbone network is composed of SIN-STEM and SIN-EDB. The SIN-STEM consists of 2D Sparse Residual Blocks (2DSRB) and SIN, which are responsible for efficient and effective feature generation. The SIN-EDB is constructed from 2DSRB, SIN, 2D Sparse encoder-decoder block (2DEDB), and AFD modules, designed to capture long-range dependencies among features.

we voxelize the point cloud following the approach of VoxelNet [5], converting the point cloud into a regular voxel grid. We use H , W , and L to denote the height, width, and length of the entire voxel space, respectively. A batch of point clouds represented as voxels is denoted by (B, H, W, L) . This implies that each voxel coordinate lies within the range $(0, 0, 0, 0)$ to $(B-1, H-1, W-1, L-1)$. The feature of each voxel is generated using a PointNet [17] network, allowing the point cloud to be converted into a sparse tensor:

$$S = (\text{feature}, \text{indice}, \text{shape}, \text{batch}), \quad (1)$$

where feature (N^v, c) represents the voxel feature with c feature channels, indice $(N^v, 4)$ denotes the voxel coordinates $\{(b_i, h_i, w_i, l_i) | i = 0, \dots, N^v - 1\}$, shape (H, W, L) defines the dimensions of the entire voxel space, and N^v is the number of voxels.

As seen, the voxel space is represented in 3D, which increases model parameters and inference time. Therefore, we simplify the voxel space by converting the 3D voxel space into H 2D slices, represented as sparse tensors:

$$S^{2D} = (\text{feature}, \text{indice}^{2D}, \text{shape}^{2D}, \text{batch} \times H), \quad (2)$$

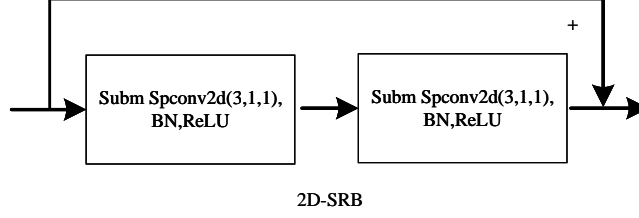


Figure 3: Detailed structure of the 2D-SRB.

where H represents the height of the original 3D voxel space, a parameter needed later in the Slice Interaction Network (SIN), $\text{shape}^{2D}(W, L)$ represents the dimensions of a 2D slice. The i -th voxel coordinates for indice^{2D} ($N^v, 3$) are defined as $(b_i^{2D}, w_i^{2D}, l_i^{2D})$, with the following transformation:

$$b_i^{2D} = b_i \times h + h_i, \quad w_i^{2D} = w_i, \quad l_i^{2D} = l_i. \quad (3)$$

Notably, since we only combine the original voxel space in the height direction (z-axis) into the batch dimension, the number of voxels N^v remains unchanged. In (3), the height of the 3D tensor is converted into the batch dimension. This slicing operation reduces the 3D point cloud representation into a 2D sparse tensor, thus reducing the data dimensionality by one. Consequently, model computation is parallelized in 2D, which reduces both the number of model parameters and inference time.

3.2.2. Sparse 2D backbone

For the transformed slice tensor, we designed a 2D feature extraction network as the backbone of the detector. This backbone network is inspired by the structure of the SAFDNet[3] model and is composed of 2D Sparse Residual Blocks (2D-SRB) (fig. 3), 2D Sparse Encoder-Decoder Blocks (2D-EDB) (fig. 4), and Adaptive Feature Diffusion (AFD). The 2D-SRB module includes a series of sparse residual blocks, each containing two 2D submanifold sparse convolutions and a skip connection linking its input and output. For the 2D-EDB module, regular sparse convolutions with a stride of 2 are used for downsampling the feature map, while sparse transposed convolutions [18] are applied for upsampling. The entire encoding-decoding process utilizes 2D

kernels. After feature extraction, the AFD structure diffuses sparse feature maps to improve the detection accuracy of the sparse detection head.

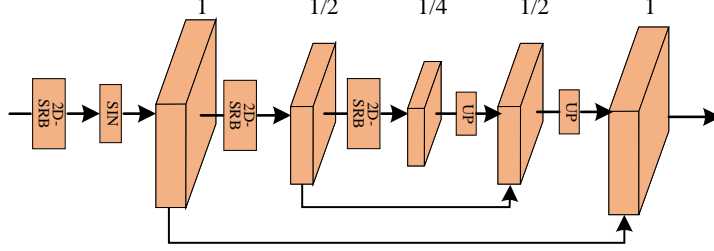


Figure 4: Composition of the SIN and 2D-EDB models, with the design of the 2D-EDB module adapted from SAFDNet [3].

3.2.3. Slice Interaction Network

Converting point clouds into slices, if processed solely as 2D slices, inevitably loses inter-slice connections, specifically the height information critical for 3D objects. As shown in table 8, the results indicate that the lack of inter-slice interaction leads to a decrease in accuracy. To address this, we propose the Slice Interaction Network (SIN). The core idea is to assemble multiple slices of the same point cloud into 3D voxels, enabling inter-slice interaction through 3D regular sparse convolutions and submanifold sparse convolutions.

Before inputting multiple slices into the network, these slices need to be transformed into 3D voxels, a process represented by the following formula. Given a batch of 2D slice S^{2D} , the corresponding 3D voxel representation is eq. (1). The coordinate of the i -th voxel is:

$$indice_i = \left(b_i^{2D} \left\lfloor \frac{1}{H} \right\rfloor, b_i^{2D} \bmod H, w_i, l_i \right). \quad (4)$$

Since regular sparse 3D convolution (spconv3d) has demonstrated strong performance and simplicity in prior research [3, 2], we incorporate three spconv3d modules with kernel size = 3 and stride = 2 as SIN modules in the 2D-SRB stage. In the 2D-EDB stage, to enhance computational efficiency and ensure that input and output feature maps have identical dimensions, we use submanifold sparse 3D convolutions (subm

spconv3d) with kernel size = 3 and stride = 1 for SIN in this stage. Overall, for the SIN module design, we select the straightforward structures of regular spconv3d and subm spconv3d, which effectively facilitate information exchange across slices, thus preserving the height information essential for 3D objects.

3.2.4. Sparse detection head

In this work, we adopt the efficient sparse detection head as the final output layer. The 2D slice-based backbone, SIN module, and sparse detection head collectively constitute PointSlice. Through the transformation of point clouds into 2D slices, inter-slice information exchange, and a fully sparse detector, PointSlice demonstrates both high efficiency and precision in performance.

4. Experiments

4.1. Datasets and metrics

To validate the effectiveness of our method, we conducted experiments on the Waymo [27], nuScenes [28], and Argoverse 2 [29] datasets. For the Waymo dataset, there are 160k and 40k annotated samples for training and validation, respectively. Evaluation metrics include mean average precision (mAP) and mAP weighted by heading accuracy (mAPH), both of which are further divided into two difficulty levels: L1, representing objects with more than 5 LiDAR points, and L2, representing objects with at least 1 LiDAR point. For the nuScenes dataset, evaluation metrics include mAP and NDS, where NDS (nuScenes Detection Score) is a weighted average of mAP and five additional metrics, measuring translation, scale, orientation, velocity, and attribute errors. The evaluation metric for Argoverse 2 is mAP.

4.2. Implementations details

Our method is implemented based on OpenPCDet [30]. PointSlice uses 8 2D sparse residual blocks, with SIN modules inserted after the 2nd, 4th, and 8th residual blocks. Each SIN module is composed of an spconv with kernel size 3 and stride 2. The model also includes a single 2D sparse EDB layer, within which one SIN module is inserted, consisting of a subm spconv with kernel size 3 and stride 1. For the AFD and

Method	Vehicle AP/APH		Pedestrian AP/APH		Cyclist AP/APH		FPS	Params
	L1	L2	L1	L2	L1	L2		
PointPillar[12]	72.1/71.5	63.6/63.1	70.6/56.7	62.8/50.3	64.4/62.3	61.9/59.9	-	-
CenterPoint[13]	73.4/72.9	65.1/64.6	75.4/65.1	67.6/58.3	67.8/66.2	65.3/63.8	-	-
PillarNeXt[11]	78.4/77.9	70.3/69.8	82.5/77.1	74.9/69.8	73.2/72.2	70.6/69.6	-	-
Voxel-or-Pillar[14]	80.2/79.7	71.9/71.5	82.5/76.9	74.8/69.4	77.1/76.0	74.2/73.2	17.2	-
PillarNet-34[4]	79.1/78.6	70.9/70.5	80.6/74.0	72.3/66.2	72.3/71.2	69.7/68.7	-	-
PillarNet-18[4]	78.2/77.7	70.4/69.9	79.8/72.6	71.6/64.9	70.4/69.3	67.8/66.7	22.7	13.42M
SECOND[19]	72.3/71.7	63.9/63.3	68.7/58.2	60.7/51.3	60.6/59.3	58.3/57.0	-	-
Part-A2[20]	77.1/76.5	68.5/68.0	75.2/66.9	66.2/58.6	68.6/67.4	66.1/64.9	-	-
PV-RCNN[21]	78.0/77.5	69.4/69.0	79.2/73.0	70.4/64.7	71.5/70.3	69.0/67.8	-	-
AFDetV2[22]	77.6/77.1	69.7/69.2	80.2/74.6	72.2/67.0	73.7/72.7	71.0/70.1	-	-
CenterFormer[23]	75.0/74.4	69.9/69.4	78.0/72.4	73.1/67.7	73.8/72.7	71.3/70.2	-	-
PV-RCNN++[24]	79.3/78.8	70.6/70.2	81.3/76.3	73.2/68.0	73.7/72.7	71.2/70.2	-	-
DSVT-Voxel[25]	79.7/79.3	71.4/71.0	83.7/78.9	76.1/71.5	77.5/76.5	74.6/73.7	-	-
SWFormer[26]	77.8/77.3	69.2/68.8	80.9/72.7	72.5/64.9	-/-	-/-	-	-
VoxelNeXt[10]	78.2/77.7	69.9/69.4	81.5/76.3	73.5/68.6	76.1/74.9	73.3/72.2	-	-
FSDV1[8]	79.2/78.8	70.5/70.1	82.6/77.3	73.9/69.1	77.1/76.0	74.4/73.3	-	-
FSDv2[9]	79.8/79.3	71.4/71.0	84.8/79.7	77.4/72.5	80.7/79.6	77.9/76.8	-	-
HEDNet[2]	81.1/80.6	73.2/72.7	84.4/80.0	76.8/72.6	78.7/77.7	75.8/74.9	-	-
SAFDNet[3]	80.6/80.1	72.7/72.3	84.7/80.4	77.3/73.1	80.0/79.0	77.2/76.2	13.6	9.89M
SAFDNet [†]	80.6/80.2	72.7/72.2	85.0/80.7	77.7/73.4	79.3/78.2	76.4/75.4	13.6	9.89M
PointSlices(ours)	80.3/79.8	72.3/71.9	84.1/79.4	76.4/71.9	77.9/76.9	75.1/74.2	15.4	7.82M
PointSlices-conv5	80.4/80.0	72.5/72.1	84.3/79.7	76.8/72.4	78.3/77.3	75.5/74.5	14.6	8.43M

Table 2: Comparison of performance between pillar-based and voxel-based models on the Waymo validation set, where [†] indicates our reproduced results. FPS (frame per second) was measured on a single NVIDIA 3090 GPU with a batch size of 1. All models were trained under single-frame setting.

sparse detection head, the model adopts the same configuration as SAFDNet. Notably, for detection on the nuScenes dataset, the model employs the SparseTransFusionHead from TransFusion [7] as its detection head.

All experiments were conducted on 8 RTX 3090 GPUs with a total batch size of 16. For fair comparison, we trained PointSlice for 24 epochs, 20 epochs, and 24 epochs on the Waymo Open, nuScenes, and Argoverse 2 datasets, respectively. For the Waymo Open dataset, we set the voxel size to (0.08m, 0.08m, 0.15m) and the detection range to [-75.52m, 75.52m] in the X and Y axes, and [-2m, 4m] in the Z axis. We employed the Adam [31] optimizer with a one-cycle learning rate policy, and set the weight-decay to 0.05, and the max learning rate to 0.003; for the nuScenes dataset, the voxel size was set to (0.075m, 0.075m, 0.2m) with the detection range of [-54m, 54m] in the X and Y axes, and [-5m, 3m] in the Z axis; for the Argoverse2 dataset, the voxel size was (0.1m, 0.1m, 0.2m) and the detection range was [-200m, 200m] in the X and Y axes, and [-4m, 4m] in the Z axis.

4.3. Comparison with state-of-the-art methods

Results on Waymo Open dataset. table 2 presents the performance results of the model on the validation set. PointSlice achieves an L2 mAPH of 72.7, an improvement of +5.5% over the state-of-the-art pillar-based method, PillarNet. Compared to the leading voxel-based method, SAFDNet, our model demonstrates a 1.13 \times faster inference speed and 0.79 \times fewer parameters, with only a 1.2% decrease in L2 mAPH. Although our model exhibits a slight gap in inference speed compared to PillarNet, our approach further narrows the performance gap between voxel-based and pillar-based methods, providing new insights for future research.

Additionally, according to the method proposed in [11], increasing the convolution kernel size can improve model accuracy. Inspired by this, we further expanded the subm3d convolution kernel size in the 2D-SRB and 2D-EDB modules from 3 to 5. As shown in table 2, the experimental results demonstrate that this adjustment improved the model’s accuracy by 0.3 L2 mAPH while maintaining an inference speed of 14.6 FPS.

Results on nuScenes. As shown in table 3, PointSlice achieves state-of-the-art results

Method	NDS	mAP	Car	Truck	Bus	T.L.	C.V.	Ped.	M.T.	Bike	T.C.	B.R.
<i>Results on the validation dataset</i>												
PillarNet-18[4]	67.4	59.9	-	-	-	-	-	-	-	-	-	-
VoxelNeXt[10]	68.7	63.5	83.9	55.5	70.5	38.1	21.1	84.6	62.8	50.0	69.4	69.4
FSDv2[9]	70.4	64.7	84.4	57.3	75.9	44.1	28.5	86.9	69.5	57.4	72.9	73.6
SAFDNet[3]	71.0	66.3	87.6	60.8	78.0	43.5	26.6	87.8	75.5	58.0	75.0	69.7
PointSlice(ours)	70.9	66.7	87.9	63.8	78.3	47.8	26.0	88.1	73.7	58.0	75.8	68.1
<i>Results on the test dataset</i>												
PointPillars[12]	45.3	30.5	68.4	23.0	28.2	23.4	4.1	59.7	27.4	1.1	30.8	38.9
3DSSD[32]	56.4	42.6	81.2	47.2	61.4	30.5	12.6	70.2	36.0	8.6	31.1	47.9
CenterPoint[13]	65.5	58.0	84.6	51.0	60.2	53.2	17.5	83.4	53.7	28.7	76.7	70.9
AFDetV2[22]	68.5	62.4	86.3	54.2	62.5	58.9	26.7	85.8	63.8	34.3	80.1	71.0
PillarNet-18[4]	70.8	65.0	87.4	56.7	60.9	61.8	30.4	87.2	67.4	40.3	82.1	76.0
PillarNet-34[4]	71.4	66.0	87.6	57.5	63.6	63.1	27.9	87.3	70.1	42.3	83.3	77.2
VoxelNeXt[10]	70.0	64.5	84.6	53.0	64.7	55.8	28.7	85.8	73.2	45.7	79.0	74.6
TransFusion-L[7]	70.2	65.5	86.2	56.7	66.3	58.8	28.2	86.1	68.3	44.2	82.0	78.2
FSDv2[9]	71.7	66.2	83.7	51.6	66.4	59.1	32.5	87.1	71.4	51.7	80.3	78.7
Voxel-or-Pillar[14]	72.7	67.0	85.8	55.1	63.5	62.1	33.3	87.6	72.5	48.6	82.9	78.2
PointSlice(ours)	71.6	67.6	87.3	51.7	67.6	65.4	37.6	88.7	73.4	41.5	85.4	77.5

Table 3: Comparison of results for different models on the nuScenes dataset. ‘T.L.’, ‘C.V.’, ‘Ped.’, ‘M.T.’, ‘T.C.’, and ‘B.R.’ denote trailer, construction vehicle, pedestrian, motor, traffic cone, and barrier.

Method	mAP	FPS	Params	Speedup
SAFDNet[3]	66.3	6.4	15.74M	1.0×
PointSlice(Ours)	66.7	6.9	7.23M	1.08×

Table 4: Performance comparison of different models on the nuScenes validation set.

Method	mAP	Vehicle	Bus	Pedestrian	Stop Sign	Box Truck	Bollard	C-Barrel	Motorcyclist	MPC-Sign	Motorcycle	Bicycle	A-Bus	School Bus	Truck Cab	C-Cone	V-Trailer	Sign	Large Vehicle	Stroller	Bicyclist	Truck	MBT	Dog	Wheelchair	W-Device	W-Rider
CenterPoint[13]	22.0	67.6	38.9	46.5	16.9	37.4	40.1	32.2	28.6	27.4	33.4	24.5	8.7	25.8	22.6	29.5	22.4	6.3	3.9	0.5	20.1	22.1	0.0	3.9	0.5	10.9	4.2
HEDNet[2]	37.1	78.2	47.7	67.6	46.4	45.9	56.9	67.0	48.7	46.5	58.2	47.5	23.3	40.9	27.5	46.8	27.9	20.6	6.9	27.2	38.7	21.6	0.0	30.7	9.5	28.5	8.7
SAFDNet[3]	39.7	78.5	49.4	70.7	51.5	44.7	65.7	72.3	54.3	49.7	60.8	50.0	31.3	44.9	24.7	55.4	31.4	22.1	7.1	31.1	42.7	23.6	0.0	26.1	1.4	30.2	11.5
PointSlice(Ours)	38.7	77.7	47.8	69.8	47.8	46.0	63.6	71.1	50.5	50.2	59.6	50.5	28.9	44.4	26.1	54.8	31.9	20.8	7.6	24.8	42.2	22.7	0.0	24.3	2.9	30.5	10.1

Table 5: Comparison of results for different models on the Argoverse 2 validation set.

on the nuScenes validation set, with a mAP of 66.74. As indicated in table 4, in terms of parameter count, PointSlice has 0.45× fewer parameters than SAFDNet and achieves a 1.08× faster inference speed. On the nuScenes test dataset, our model achieved an outstanding performance of 67.6 mAP, demonstrating higher detection accuracy compared to the efficient models PillarNet-18[4] and [14].

Results on Argoverse2. To further validate our model’s detection performance in long-range and multi-class scenarios, we conducted experiments on the Argoverse 2 validation set. As shown in table 5 and table 6, the results show that PointSlice achieves an mAP of 38.7, with a 1.0% reduction in accuracy compared to the state-of-the-art SAFDNet, but with a 1.10× faster inference speed and 0.66× fewer parameters. These results further demonstrate the efficiency of our model.

Method	mAP	FPS	Params	Speedup
SAFDNet[3]	39.7	10.8	6.11M	1.0×
PointSlice(Ours)	38.2	11.9	4.05M	1.1×

Table 6: Performance comparison of different models on the Argoverse 2 validation set.

Method	mAPH(L2)	Params	Speedup	FPS
SAFDNet	73.9	9.89M	1.0×	13.68
SAFD-Pillar	69.3	7.74M	1.17×	15.95
PointSlice	72.7	7.82M	1.13×	15.40

Table 7: Ablation study of different point cloud processing methods on the Waymo validation set.

Method	mAPH(L2)	Params
(2D-STEM,2D-EDB)	71.5	7.62M
(2D-STEM+SIN,2D-EDB)	72.5	7.71M
(2D-STEM,2D-EDB+SIN)	71.9	7.73M
(2D-STEM+SIN,2D-EDB+SIN)	72.7	7.82M

Table 8: Ablation study of applying SIN at different positions in PointSlice on the Waymo validation set.

4.4. Ablation studies

To validate the effectiveness of the PointSlice model over the pillar-based approach in point cloud processing, as well as the contribution of the SIN module, we conducted ablation experiments on the Waymo dataset.

Comparison between slice and pillar approaches. To ensure variable consistency, our comparison isolates the difference in point cloud processing methods. We keep the 2D feature map dimensions, the number of dimensions, and the quantity of SRB and EDB modules consistent between both methods. SAFDNet-pillar denotes a configuration where each voxel size is set to $[0.08, 0.08, 6]$, allowing us to observe the performance of SAFDNet under pillar-based processing. As shown in table 7, PointSlice achieves a higher accuracy of +3.4% mAP compared to SAFDNet-pillar while maintaining similar inference speed. This demonstrates that the slice approach provides more precise results than pillar processing for point clouds, while also preserving model efficiency.

Comparison of SIN Modules. To demonstrate the role of SIN in PointSlice, we conducted three comparative experiments, as shown in table 8. The first row indicates that

Model	Memory-Inference		
	Waymo	nuScenes	Argoverse 2
SAFDNet[3]	410MB	905MB	273MB
PointSlice	264MB	860MB	188MB

Table 9: Comparison of Model GPU Memory Usage on Different Datasets. For all experiments, the batch size is set to 1.

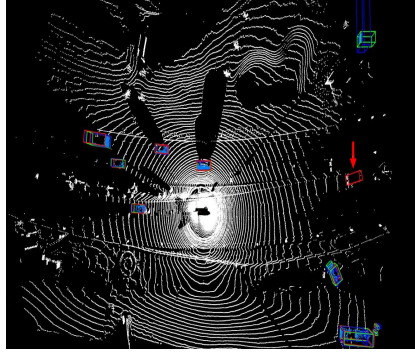
the SIN module is not included in the PointSlice network, while the second row represents the insertion of the SIN module only in the 2D-STEM. A comparison of these two results shows that adding the SIN module improves the model’s accuracy by 1.0%, indicating that SIN indeed facilitates feature interaction across slices. The third row indicates that adding the SIN module solely within the 2D-EDB module results in a 0.4 improvement in performance compared to the first row without SIN. The fourth row represents the model with the SIN module integrated into both the 2D-STEM and 2D-EDB modules, achieving the best performance with an mAPH of 72.7. This demonstrates that the SIN module plays a crucial role in enhancing both the 2D-STEM and 2D-EDB modules.

Comparison of Memory Usage During Model Inference. We conducted experiments to evaluate GPU memory consumption of different models on various datasets. To measure memory usage, we utilized `torch.cuda.max_memory_allocated()`.

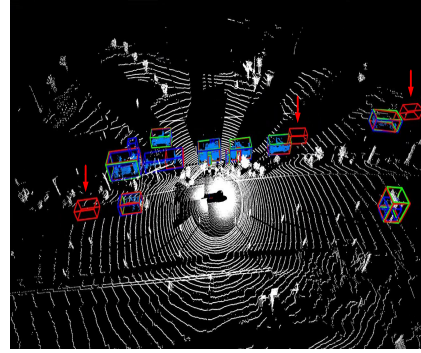
The experimental results are shown in table 9. From the table, it can be observed that on the Waymo, nuScenes, and Argoverse 2 datasets, the memory consumption of our PointSlice model is only 0.64 times, 0.95 times, and 0.69 times that of the SAFDNet model, respectively. This demonstrates the efficiency and lightweight characteristics of our proposed model.

4.5. Qualitative visualization

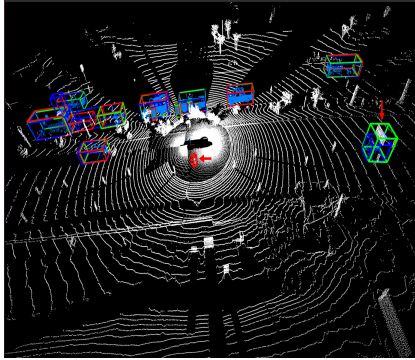
As shown in the fig. 5, we compared the visualization results of PointSlice and SAFDNet-pillar on the Waymo validation dataset. The visualization results indicate that our model demonstrates superior performance in terms of detection accuracy,



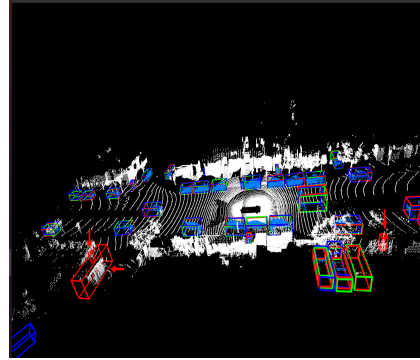
(a) Image(1)



(b) Image(136)



(c) Image(141)



(d) Image(4066)

Figure 5: Qualitative results on Waymo. The blue, red, and green boxes are human annotations, SAFDNet-Pillar predictions and PointSlice predictions, respectively. The blue points denote the points that fall within the human-annotated boxes. Compared to SAFDNet-pillar, PointSlice demonstrates superior accuracy in object identification and exhibits more effective detection in reducing false positives. In the point cloud visualization process, the score threshold is set to 0.3, and the non-maximum suppression (NMS) threshold is set to 0.1. Red arrows mark the prediction differences.

whereas the SAFDNet-pillar network exhibits issues with false positive object detections.

5. Conclusion

In summary, to overcome the challenges of low inference efficiency in voxel-based models and reduced detection accuracy in pillar-based models, we developed a horizontal slicing approach for 3D point cloud data. This method effectively reduces the computational burden of voxel-based models. Additionally, we introduced the Slice Interaction Network (SIN) to facilitate feature interaction across slices, resulting in the PointSlice model. Evaluation on the Waymo, nuScenes, and Argoverse 2 datasets demonstrates that PointSlice achieves both high efficiency and high accuracy, validating the effectiveness of our approach.

References

- [1] Y. Zhu, R. Mottaghi, E. Kolve, J. J. Lim, A. Gupta, L. Fei-Fei, A. Farhadi, Target-driven visual navigation in indoor scenes using deep reinforcement learning, in: 2017 IEEE international conference on robotics and automation (ICRA), IEEE, 2017, pp. 3357–3364.
- [2] G. Zhang, C. Junnan, G. Gao, J. Li, X. Hu, Hednet: A hierarchical encoder-decoder network for 3d object detection in point clouds, *Advances in Neural Information Processing Systems* 36 (2024).
- [3] G. Zhang, J. Chen, G. Gao, J. Li, S. Liu, X. Hu, Safdnet: A simple and effective network for fully sparse 3d object detection, in: *Proceedings of the IEEE/CVF Conference on Computer Vision and Pattern Recognition*, 2024, pp. 14477–14486.
- [4] G. Shi, R. Li, C. Ma, Pillarnet: Real-time and high-performance pillar-based 3d object detection, in: *European Conference on Computer Vision*, Springer, 2022, pp. 35–52.

- [5] Y. Zhou, O. Tuzel, Voxelnet: End-to-end learning for point cloud based 3d object detection, in: Proceedings of the IEEE conference on computer vision and pattern recognition, 2018, pp. 4490–4499.
- [6] J. Deng, S. Shi, P. Li, W. Zhou, Y. Zhang, H. Li, Voxel r-cnn: Towards high performance voxel-based 3d object detection, in: Proceedings of the AAAI conference on artificial intelligence, Vol. 35, 2021, pp. 1201–1209.
- [7] X. Bai, Z. Hu, X. Zhu, Q. Huang, Y. Chen, H. Fu, C.-L. Tai, Transfusion: Robust lidar-camera fusion for 3d object detection with transformers, in: Proceedings of the IEEE/CVF conference on computer vision and pattern recognition, 2022, pp. 1090–1099.
- [8] L. Fan, F. Wang, N. Wang, Z.-X. Zhang, Fully sparse 3d object detection, Advances in Neural Information Processing Systems 35 (2022) 351–363.
- [9] L. Fan, F. Wang, N. Wang, Z. Zhang, Fsd v2: Improving fully sparse 3d object detection with virtual voxels, arXiv preprint arXiv:2308.03755 (2023).
- [10] Y. Chen, J. Liu, X. Zhang, X. Qi, J. Jia, Voxelnext: Fully sparse voxelnet for 3d object detection and tracking, in: Proceedings of the IEEE/CVF Conference on Computer Vision and Pattern Recognition, 2023, pp. 21674–21683.
- [11] J. Li, C. Luo, X. Yang, Pillarnext: Rethinking network designs for 3d object detection in lidar point clouds, in: Proceedings of the IEEE/CVF Conference on Computer Vision and Pattern Recognition, 2023, pp. 17567–17576.
- [12] A. H. Lang, S. Vora, H. Caesar, L. Zhou, J. Yang, O. Beijbom, Pointpillars: Fast encoders for object detection from point clouds, in: Proceedings of the IEEE/CVF conference on computer vision and pattern recognition, 2019, pp. 12697–12705.
- [13] T. Yin, X. Zhou, P. Krahenbuhl, Center-based 3d object detection and tracking, in: Proceedings of the IEEE/CVF conference on computer vision and pattern recognition, 2021, pp. 11784–11793.

- [14] Y. Huang, S. Zhou, J. Zhang, J. Dong, N. Zheng, Voxel or pillar: Exploring efficient point cloud representation for 3d object detection, in: Proceedings of the AAAI Conference on Artificial Intelligence, Vol. 38, 2024, pp. 2426–2435.
- [15] B. Graham, L. Van der Maaten, Submanifold sparse convolutional networks, arXiv preprint arXiv:1706.01307 (2017).
- [16] B. Graham, Sparse 3d convolutional neural networks, arXiv preprint arXiv:1505.02890 (2015).
- [17] C. R. Qi, H. Su, K. Mo, L. J. Guibas, Pointnet: Deep learning on point sets for 3d classification and segmentation, in: Proceedings of the IEEE conference on computer vision and pattern recognition, 2017, pp. 652–660.
- [18] Spconv Contributors, Spconv: Spatially sparse convolution library, <https://github.com/traveller59/spconv>, accessed: 2022-03 (2022).
- [19] Y. Yan, Y. Mao, B. Li, Second: Sparsely embedded convolutional detection, Sensors 18 (10) (2018) 3337.
- [20] S. Shi, Z. Wang, J. Shi, X. Wang, H. Li, From points to parts: 3d object detection from point cloud with part-aware and part-aggregation network, IEEE transactions on pattern analysis and machine intelligence 43 (8) (2020) 2647–2664.
- [21] S. Shi, C. Guo, L. Jiang, Z. Wang, J. Shi, X. Wang, H. Li, Pv-rcnn: Point-voxel feature set abstraction for 3d object detection, in: Proceedings of the IEEE/CVF conference on computer vision and pattern recognition, 2020, pp. 10529–10538.
- [22] Y. Hu, Z. Ding, R. Ge, W. Shao, L. Huang, K. Li, Q. Liu, Afdetv2: Rethinking the necessity of the second stage for object detection from point clouds, in: Proceedings of the AAAI Conference on Artificial Intelligence, Vol. 36, 2022, pp. 969–979.
- [23] Z. Zhou, X. Zhao, Y. Wang, P. Wang, H. Foroosh, Centerformer: Center-based transformer for 3d object detection, in: European Conference on Computer Vision, Springer, 2022, pp. 496–513.

- [24] S. Shi, L. Jiang, J. Deng, Z. Wang, C. Guo, J. Shi, X. Wang, H. Li, Pv-rcnn++: Point-voxel feature set abstraction with local vector representation for 3d object detection, *International Journal of Computer Vision* 131 (2) (2023) 531–551.
- [25] H. Wang, C. Shi, S. Shi, M. Lei, S. Wang, D. He, B. Schiele, L. Wang, Dsvt: Dynamic sparse voxel transformer with rotated sets, in: *Proceedings of the IEEE/CVF Conference on Computer Vision and Pattern Recognition*, 2023, pp. 13520–13529.
- [26] P. Sun, M. Tan, W. Wang, C. Liu, F. Xia, Z. Leng, D. Anguelov, Swformer: Sparse window transformer for 3d object detection in point clouds, in: *European Conference on Computer Vision*, Springer, 2022, pp. 426–442.
- [27] P. Sun, H. Kretzschmar, X. Dotiwalla, A. Chouard, V. Patnaik, P. Tsui, J. Guo, Y. Zhou, Y. Chai, B. Caine, et al., Scalability in perception for autonomous driving: Waymo open dataset, in: *Proceedings of the IEEE/CVF conference on computer vision and pattern recognition*, 2020, pp. 2446–2454.
- [28] H. Caesar, V. Bankiti, A. H. Lang, S. Vora, V. E. Liong, Q. Xu, A. Krishnan, Y. Pan, G. Baldan, O. Beijbom, nuscenes: A multimodal dataset for autonomous driving, in: *Proceedings of the IEEE/CVF conference on computer vision and pattern recognition*, 2020, pp. 11621–11631.
- [29] B. Wilson, W. Qi, T. Agarwal, J. Lambert, J. Singh, S. Khandelwal, B. Pan, R. Kumar, A. Hartnett, J. K. Pontes, et al., Argoverse 2: Next generation datasets for self-driving perception and forecasting, *arXiv preprint arXiv:2301.00493* (2023).
- [30] O. D. Team, OpenPCDet: An open-source toolbox for 3d object detection from point clouds, <https://github.com/open-mmlab/OpenPCDet>, accessed: 2020-06 (2020).
- [31] D. P. Kingma, Adam: A method for stochastic optimization, *arXiv preprint arXiv:1412.6980* (2014).

- [32] Z. Yang, Y. Sun, S. Liu, J. Jia, 3dssd: Point-based 3d single stage object detector, in: Proceedings of the IEEE/CVF conference on computer vision and pattern recognition, 2020, pp. 11040–11048.